

Cite this: *Lab Chip*, 2011, **11**, 1359

www.rsc.org/loc

PAPER

## High-throughput cell cycle synchronization using inertial forces in spiral microchannels†

Wong Cheng Lee,<sup>ab</sup> Ali Asgar S. Bhagat,<sup>a</sup> Sha Huang,<sup>c</sup> Krystyn J. Van Vliet,<sup>ade</sup> Jongyoon Han<sup>\*ace</sup> and Chwee Teck Lim<sup>\*abfg</sup>

Received 10th November 2010, Accepted 21st January 2011

DOI: 10.1039/c0lc00579g

Efficient synchronization and selection of cells at different stages of the cell replication cycle facilitates both fundamental research and development of cell cycle-targeted therapies. Current chemical-based synchronization methods are unfavorable as these can disrupt cell physiology and metabolism. Microfluidic systems developed for physical cell separation offer a potential alternative over conventional cell synchronization approaches. Here we introduce a spiral microfluidic device for cell cycle synchronization, using the combined effects of inertial forces and Dean drag force. By exploiting the relationship between cell diameter and cell cycle (DNA content/ploidy), we have successfully fractionated several asynchronous mammalian cell lines, as well as primary cells comprising bone marrow-derived human mesenchymal stem cells (hMSCs), into enriched subpopulations of G0/G1 (>85%), S, and G2/M phases. This level of cell cycle enrichment is comparable to existing microfluidic systems, but the throughput ( $\sim 15 \times 10^6$  cells per h) and viability ( $\sim 95\%$ ) of cells thus synchronized are significantly greater. Further, this platform provides rapid collection of synchronized cells or of diameter-sorted cells post-separation, to enable diverse applications in the study and manipulation of cell proliferation.

### Introduction

Cell cycle synchronization is essential for studying cellular properties, biological processes and elucidating genetic regulatory mechanisms and events involved in each phase prior to cell division. In eukaryotic cells, the distinct events leading to proper cell division can be separated into four sequential phases: G1 (gap), S (DNA synthesis), G2 (gap) and M (mitosis). As a cell progresses through the cell cycle, it duplicates its chromosomes during the S phase and segregates the chromosomes in the M phase. The use of a highly synchronized population of cells has

facilitated the development of a variety of biological systems. For example, *via* such synchronization of cancer cells, several key oncogenes have been identified and implicated in specific cell cycle checkpoints.<sup>1</sup> Development of cancer therapeutics has thus employed tumor cell synchronization, because anticancer drugs are known to target cells in different phases of the cell cycle.<sup>2,3</sup> In stem cell therapies that involve nuclear transfer to the host cells, cell cycle synchronization is critical because stem cells in the G0/G1 phase impart higher nuclear transfer efficiency.<sup>4</sup> Thus, there is great interest in developing efficient techniques to rapidly synchronize and to isolate cells at various phases of the cell cycle.

Typically, cells are synchronized by inhibiting DNA replication in the S phase, *via* methods including addition of chemicals such as hydroxyurea, methotrexate or aphidicolin to the culture media.<sup>5</sup> Synchronized cultures of G0/G1 phase can also be obtained by withdrawal of growth factors and specific amino acids termed “serum starvation”<sup>6</sup> or growing the cells at very high density to achieve “contact inhibition” for non-transformed cell lines.<sup>7</sup> Although these techniques have the ability to obtain large numbers of synchronized dividing cells, the metabolism and biochemical balance within the cells are often altered, leading to unbalanced growth of cells and disrupted progression through the cell cycle. In severe cases, the metabolic agent reduces cell viability and promotes apoptosis.<sup>8,9</sup> Other synchronization techniques also rely on separation of cells at specific cell cycle stages, including fluorescence-activated cell sorting (FACS) and counter-flow centrifugal elutriation (CCE). In FACS, cells with

<sup>a</sup>BioSystems and Micromechanics (BioSyM) IRG, Singapore-MIT Alliance for Research and Technology (SMART) Centre, Singapore. E-mail: jyhan@mit.edu

<sup>b</sup>NUS Graduate School for Integrative Sciences and Engineering, National University of Singapore, Singapore. E-mail: ctim@nus.edu.sg

<sup>c</sup>Department of Electrical Engineering & Computer Science, Massachusetts Institute of Technology, Room 36-841, 77 Massachusetts Avenue, Cambridge, MA, USA

<sup>d</sup>Department of Materials Science and Engineering, Massachusetts Institute of Technology, Cambridge, MA, USA

<sup>e</sup>Department of Biological Engineering, Massachusetts Institute of Technology, Cambridge, MA, USA

<sup>f</sup>Division of Bioengineering and Department of Mechanical Engineering, National University of Singapore, 7 Engineering Drive 1, Singapore, 117574, Singapore

<sup>g</sup>Mechanobiology Institute, National University of Singapore, Singapore

† Electronic supplementary information (ESI) available. See DOI: 10.1039/c0lc00579g

similar fluorescence signal intensity (*i.e.* DNA content) or light scattering characteristics (size) can be sorted rapidly yielding a relatively pure population of synchronized cells. However, the viability of the cells is usually compromised with very poor recovery of cells for subsequent assays.<sup>10</sup> In CCE, cells are synchronized by taking advantage of the relationship between a cell volume (size) and its phase in the cell cycle. This allows the proliferating unsynchronized cell population to be synchronized in the different phases.<sup>11</sup> During elutriation, the smaller cells elute first from the chamber followed by the larger cells. Thus, the early elution is comprised mainly of cells in the G0/G1 phase of the cell cycle while the S and G2/M cells are eluted subsequently. This method yields cell populations with the highest synchrony in the G1 phase and moderate dispersion of synchrony, especially for S and G2/M phases. Unlike chemical and growth limiting methods, centrifugal elutriation does not affect the metabolism of cells, but requires large capital investment, large cell numbers for sufficient signal/noise ratios, and imposes significant mechanical stress on the cells.<sup>12</sup>

Microfabricated cell separation systems offer considerable advantages over conventional cell sorting approaches, including reduced sample volume, reduced sample preparation procedures, higher sample throughput, and high spatial resolution.<sup>13</sup> Microfluidic devices for cell cycle synchronization and separation have been reported recently, using active separation techniques such as dielectrophoresis<sup>14</sup> and acoustophoresis.<sup>15</sup> Although such devices are powerful tools for size-based cell separation, they often involve complex and costly setups, and the use of active energy sources for separation could potentially affect the cell viability. Passive separation techniques using hydrophoresis<sup>16</sup> and hydrodynamic filtration<sup>17</sup> for cell cycle synchronization have also been demonstrated, but the low throughput of these methods has limited adoption by the biological community. Hence there is a clear need to develop a simple, high throughput, and high purity technique for cell cycle synchronization, with minimal perturbation to cell physiology.

In this work, we present a microfluidics based approach to synchronize cells using inertial forces in spiral microchannels. Recently, size based particle separation in microfluidic systems has been developed based on the principles of inertial migration.<sup>18,19</sup> In spiral shaped microchannels, under the Poiseuille flow condition, particles of varying sizes equilibrate at distinct positions along the microchannel cross-section under the influence of inertial lift and Dean drag forces. Using this principle, we have successfully synchronized several mammalian permanent cell lines, including Chinese Hamster Ovarian Cells (CHO-CD36) and cancer cells (HeLa and K KU-100) into populations enriched in G0/G1 (>85%), S and G2/M phase cells. The separation principle exploits the relationship between a cell volume (and thus diameter or, more generically, “size”) and its phase in the cell cycle: to maintain the same average cell size over many such cycles, each cell will approximately double in volume before it divides. We also demonstrate here the first application of this technique to synchronize primary bone marrow-derived human mesenchymal stem cells (hMSCs). Our results indicate that the G0/G1 to G2/M ratio of 2.8 : 1 of the asynchronous sample is enriched to 15.7 : 1. Similarly, a fourfold enrichment in the G2/M population is achieved post-synchronization. These

results are comparable with those reported using other microfluidic systems<sup>14–17</sup> but afford significantly increased throughput ( $\sim 15 \times 10^6$  cells per h) of synchronized cells maintaining high viability ( $\sim 95\%$ ). We believe that the passive operating principle, coupled with the simple microchannel design, will enable diverse applications requiring high-throughput and low-cost synchronization of primary cells.

## Materials and methods

### Cell culture

Human bone marrow-derived mesenchymal stromal or stem cells (hMSCs; Lonza, Switzerland) were cultured in low-glucose Dulbecco's modified Eagle's medium (DMEM) (Invitrogen, USA) supplemented with 10% fetal bovine serum (FBS) (Invitrogen, USA) together with 1% penicillin–streptomycin (Invitrogen, USA). Chinese hamster ovary cells transfected with human CD36, or CHO-CD36 (ATCC, USA), were cultured in RPMI 1640 medium (Invitrogen, USA) supplemented with 10% FBS together with 1% penicillin–streptomycin. Cervical cancer cells HeLa (CCL-2™, ATCC, USA) were cultured in low-glucose DMEM supplemented with 10% FBS and 1% penicillin–streptomycin. The cholangiocarcinoma cell line, K KU-100, was cultured in Ham's F-12 medium containing 10% FBS, 3% HEPES buffer and 1% penicillin–streptomycin. All cultures were maintained at 37 °C in a humidified atmosphere containing 5% (v/v) CO<sub>2</sub>. The hMSCs were seeded at 500 cells per cm<sup>2</sup> and cultured in sterile 175 cm<sup>2</sup> flasks (Corning) and dissociated after 48 hours with 0.01% trypsin and 5.3 mM EDTA to prevent contact inhibition. The CHO-CD36, HeLa and K KU-100 cell lines were cultured in sterile 25 cm<sup>2</sup> flasks (Corning) and subcultivated (1 : 4) three times a week; media was replaced every 48 h. Subconfluent monolayers were dissociated with 0.01% trypsin and 5.3 mM EDTA.

Prior to spiral microfluidics-based experiments, the asynchronous cells were diluted to 100 000 cells per mL in buffer containing 1× phosphate buffered saline (PBS), 2 mM ethylenediaminetetraacetic acid (EDTA) supplemented with 1% bovine serum albumin (BSA) (Miltenyi Biotec, Germany) to prevent agglomeration and adsorption to the microchannel walls. The solution density was adjusted to prevent cell sedimentation by supplementing with 3.5% w/v dextran 40 (Appli-Chem Asia, Singapore).

To initiate G1 arrest by contact inhibition, hMSCs were seeded at 20 000 cells per cm<sup>2</sup> and cultured in DMEM supplemented with 10% FBS for 48 h. For G1 arrest by serum starvation, hMSCs were seeded at 500 cells per cm<sup>2</sup> and cultured in DMEM without FBS for 48 h. The G1-arrested cells were dissociated with 0.01% trypsin and 5.3 mM EDTA solution before fixing in 70% ethanol for 30 min.

### Microchannel fabrication and characterization

Devices were fabricated in polydimethylsiloxane (PDMS, Sylgard 184, Dow Corning, USA) using standard soft-lithographic techniques (Fig. 2a).<sup>20</sup> Briefly, 6 inch-diameter silicon wafers were first patterned and etched using deep reactive ion etching (DRIE) to define the channels on the wafer. Following etching, the patterned silicon wafers were treated with trichloro

(1H,1H,2H,2H-perfluorooctyl) silane (Sigma Aldrich, USA) for 2 h to facilitate PDMS mold release. Following silanization, PDMS prepolymer, mixed at a 10 : 1 (w/w) ratio with a curing agent, was poured on the silicon master and cured at 70 °C for 2.5 h. The cured PDMS mold was then peeled from the silicon wafer to serve as a master template for subsequent PDMS casting. Next, the PDMS template was silanized for 2 h to aid release of subsequent PDMS molds. Note that surface roughness due to DRIE of the Si master surface and PDMS replication results in channel wall surface roughness on the order of 1 μm; flow fields in channel dimensions of >200 μm are thus minimally affected by surface roughness.<sup>21</sup> Following curing and peeling on the final PDMS molds with the desired microchannel patterns, holes for inlet and outlets were punched using 1.5 mm-diameter biopsy punch. The PDMS molds were then irreversibly bonded to microscopic glass slides (1 in. × 3 in. × 1 mm; Fisher Scientific Inc., USA) using oxygen plasma treatment (Covance, Femto Science, South Korea).

Fluorescent polystyrene beads of varying diameter (25 μm—green, 15 μm—blue and 10 μm—red) (ITS Science & Medical, Singapore) were suspended in equal proportions in 1 × PBS and 3.5 (w/v) dextran 40 with 1% BSA at a total concentration of  $1.2 \times 10^5$  beads per mL. To characterize the spiral microfluidic device, the bead mixtures and cell suspensions were filled in a 60 mL syringe and injected into the microchannel using a syringe pump (NE-1000, New Era Pump Systems Inc., USA) driven at a flowrate of 2.5 mL min<sup>-1</sup>. Flow was experimentally observed under an inverted epi-fluorescence microscope (Olympus IX81, Olympus Inc., USA) equipped with a 12-bit EMCCD camera (iXon<sup>EM</sup> + 885, Andor Technology, USA). Following testing, optical microscopy images of the cell populations collected from each outlet were acquired within a hemocytometer, and the cell diameter calculated from the photographs using Metamorph<sup>®</sup> software (Molecular Devices, USA).

### Cell cycle analysis

Flow cytometry analysis was conducted on the sorted samples to analyze the cellular DNA content *via* propidium iodide (PI).<sup>22</sup> The sorted, synchronized cell populations were rinsed in 1 × PBS and fixed in 70% ethanol for 30 min at 4 °C. Cells were then centrifuged at 600 g for 5 min and incubated for 30 min in the staining solution containing 1 × PBS, 3.8 mM sodium citrate (Sigma Aldrich, USA), 10 μg mL<sup>-1</sup> RNase (i-DNA Biotechnology, Singapore) and 50 μg mL<sup>-1</sup> propidium iodide (Sigma Aldrich, USA). The stained cells were then tested for synchronization efficiency by performing flow cytometry (BD<sup>™</sup> LSR II flow cytometer, BD Biosciences, USA), and gated data were analyzed *via* Cyflogic (CyFlo Ltd, Finland) software.

## Results and discussion

### Design principle

Fig. 1 shows a schematic illustration of the spiral microfluidic separators. Size-based cell separations using inertial forces in microfluidic systems have gained interest in recent times due to the high separation resolution combined with high throughput (in cells per hour). Continuous size-based separation using the

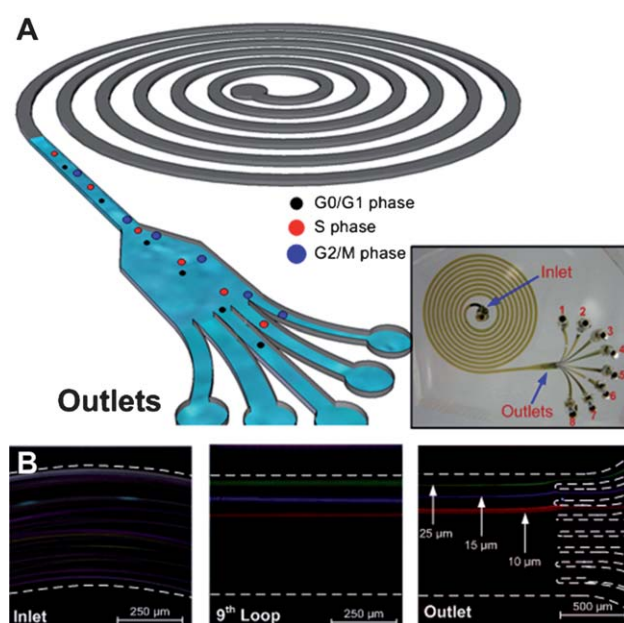


**Fig. 1** (A) Schematic illustration of the spiral microfluidic design developed for cell cycle synchronization. Under the influence of inertial lift forces and Dean drag force, asynchronous cell populations are size fractionated to obtain relatively pure populations of cells in the G0/G1, S and G2/M phase. The cells in the G2/M phase, due to the larger diameter at this cell cycle stage, equilibrate closest to the microchannel inner wall followed by cells in the S and the G0/G1 phase. Inset: photograph of the spiral microchannel with one inlet and eight outlets fabricated in PDMS. (B) Validation of design principle using fluorescently labeled polystyrene particles. Superimposed images illustrating distribution and position of the 10 μm, 15 μm, and 25 μm diameter particles at the inlet, a 500 μm wide channel section prior to the outlet, and the bifurcated outlet of a 140 μm high microchannel at 2.5 mL min<sup>-1</sup> flowrate. The randomly distributed particles at the inlet form ordered focused streams which are then collected separately at outlets 1 (largest), 2 and 3 (smallest).

combined effect of inertial lift forces and the Dean force was applied by Kuntaegowdanahalli *et al.* for the separation of 10 μm, 15 μm and 20 μm particle diameters in a single pass, and for the separation of SH-SY5Y neuroblastoma and C6 rat glioma cell lines.<sup>23</sup> Russom *et al.* further applied this technique to achieve leukocyte enrichment in blood.<sup>24</sup> In this work, we adapted this principle for the synchronization of cells based on their phase in the cell cycle. The device achieves cell cycle synchronization by exploiting the relationship between cell volume (and thus the general size or specific diameter) and phase within the cell cycle. We have size fractionated human mesenchymal stem cells (hMSCs) into synchronized populations of G0/G1, S and G2/M phase cells.

Detailed discussion of the device operating principle is available elsewhere.<sup>23</sup> Briefly, in simple particle-laden tube flows under Poiseuille flow conditions, balance between the shear-induced and wall-induced lift forces equilibrates the suspended particles in an annular fashion around the tube periphery, and is termed the “tubular pinch” effect.<sup>25–27</sup> In channels with rectangular cross-sections the lift force ( $F_L$ ) equilibrates the particles at eight distinct positions across the channel cross-section.<sup>28</sup> This lift force ( $F_L$ ) is very sensitive to the particle size ( $F_L \propto d^4$ , where  $d$  is the particle diameter) and recent studies have shown that for

$d/D \geq 0.07$ , where  $D$  is the microchannel diameter, these inertial lift forces are significantly larger and result in particle equilibration within short distances; ideal for separation *via* microfluidic systems.<sup>18,19,29,30</sup> Further, in low aspect ratio rectangular microchannels, the microchannel diameter  $D$  can be approximated by the microchannel height ( $H$ ).<sup>31</sup>

In spiral shaped microchannels, particles flowing are subjected to both the inertial lift forces and the Dean drag force. The outward directed centrifugal force in curvilinear channels gives rise to counter rotating vortices, also known as Dean vortices, in the top and bottom half of the microchannel. These secondary Dean vortices exert a drag force on the suspended particles, entraining them within the vortex. The magnitude of this Dean drag force ( $F_D$ ) varies with the particle diameter and its position within the channel cross-section ( $F_D \propto d$ ).<sup>32</sup> The interplay between the inertial lift force ( $F_L$ ) and the Dean drag force ( $F_D$ ) reduces the eight equilibrium positions to just two positions near the inner channel wall, each within the top and bottom Dean vortex.<sup>24</sup> The two equilibrium positions overlay each other along the microchannel height and are located at the same distance from the microchannel inner wall for a given particle size, *i.e.*, viewed as a single position across the microchannel width (Fig. 1b). As this focusing position is dependent on both  $F_L$  and  $F_D$ , it varies significantly with the particle diameter ( $F_L/F_D \propto d^3$ ). This implies that particles of different sizes occupy different lateral positions within the microchannel cross-section, with the largest particle being focused closest to the inner channel wall.<sup>23</sup>

To corroborate the design principle and determine the flow conditions, a mixture of 25  $\mu\text{m}$ , 15  $\mu\text{m}$  and 10  $\mu\text{m}$ -diameter fluorescently labeled polystyrene beads were tested through the spiral microchannel. These bead diameters were chosen to mimic the size range of mammalian cells. The microchannel design consisted of 9-loop spiral geometry (length  $\sim 40$  cm) with single inlet and eight bifurcating outlets. The microchannel width was fixed at 500  $\mu\text{m}$  and the height was varied to satisfy the  $d/D > 0.07$  ratio for the different cell types. The spiral diameter and the microchannel lengths were calculated to allow all the particles/cells to equilibrate under the influence of the lift forces.<sup>32</sup> Fig. 1b presents superimposed fluorescent images of the microbeads captured at the inlet and outlet of the microchannel at an optimized flowrate of 2.5  $\text{mL min}^{-1}$ . By the time the flowstream reached the outlet, the beads of three distinct diameters were focussed into three distinct streams across the microchannel cross-section; these bead subpopulations were efficiently collected at outlet 1, 2 and 3, respectively.

### Synchronization of permanent cultures

In an exponentially growing mammalian culture, cells having just entered the G1 phase exhibit diameters at the lower end of the population distribution.<sup>33</sup> As the cells achieve a critical size through protein and lipid synthesis, the cells initiate a new cell cycle in late G1 phase and synthesize DNA in the S phase. Cell growth continues until mitosis (M phase), at which point the cell volume increases to approximately twice the original volume in G0/G1 phase. Correspondingly, cells in the G2/M phase have two copies of DNA.

We first investigated the synchronization performance of the device using two cancer cell lines, HeLa and K KU-100 cells. As

the mean diameter of the HeLa and K KU-100 cell population was measured as  $d = 16.3 \pm 2.5$   $\mu\text{m}$  and  $16.9 \pm 3.1$   $\mu\text{m}$ , respectively, each cell line was sorted separately using a 140  $\mu\text{m}$ -high spiral microchannel (satisfying  $d/H \geq 0.07$ ). When the cells were introduced into the microchannel, the asynchronous cells exhibiting an initially broad size distribution were separated into distinct trajectories at different lateral positions along the inner half of the microchannel. After sorting, the diameters of the unsorted (control) and sorted cells collected from outlets 1–4 were analyzed *via* optical microscopy (see Methods section). Results indicate that the cells were successfully separated on the basis of their size. For both cell line types, the cell subpopulations of largest diameter were collected in the outlet closest to the inner microchannel walls (outlet 1) with mean diameters of  $19.4 \pm 5.6$   $\mu\text{m}$  (HeLa) and  $24.6 \pm 3.0$   $\mu\text{m}$  (K KU-100) (see Fig. S1, ESI†). The HeLa and K KU-100 cell subpopulations of smallest diameter were collected in outlet 4 with mean diameters of  $13.5 \pm 1.5$   $\mu\text{m}$  and  $16.6 \pm 2.4$   $\mu\text{m}$ , respectively (see Fig. S1, ESI†). Similarly, another cell line, CHO-CD36 cells, was also size fractionated using a 200  $\mu\text{m}$  high microchannel to accommodate the larger size distribution of this genetically engineered cell line (13.3–36.7  $\mu\text{m}$ ) (see Fig. S1, ESI†).

Cells in different phases of the cell cycle can be distinguished by the amount of cellular DNA content. The distributions of cell cycle phases in these size-fractionated lines were estimated using flow cytometric analysis of DNA fluorescence intensity *via* propidium iodide (see Methods section). As noted, cells in the G2/M phase typically exhibit twice the DNA fluorescence intensity as compared to cells in the G0/G1 phase. The percentage of cells in each phase was calculated, and doublet and aggregate cells were eliminated *via* comparison of fluorescent area and width plots.<sup>22</sup> Fig. 2 presents histograms indicating the distribution of the DNA content of the sorted (singlet) cells in the G0/G1, S and G2/M phase after synchronization for the HeLa, K KU-100 and CHO-CD36 cell lines. The CHO-CD36 cells show a larger size distribution ( $19.1 \pm 5.3$   $\mu\text{m}$ ) as the cells pass through their cell cycle compared to the cancer cells. As the device separates cells based on their size, the CHO-CD36 cells are thus fractionated (synchronized) more efficiently in the G2/M phase than the cancer cell lines. Following separation, high synchrony of cells was achieved in cells collected from outlet 4 with 84% of HeLa, 96% of K KU-100 and 86% of CHO-CD36 cells synchronized in the G0/G1 phase. Concurrently, an enrichment of two- to threefold in G2/M phase was achieved in cells collected from outlet 1 (Table 1). These results are comparable with those reported using other microfluidic systems.<sup>14–17</sup> However, the high flow throughput of the present approach can fractionate  $\sim 15 \times 10^6$  cells per h, which is at least fivefold higher than that reported previously for other microfluidics-based methods. The passive sorting principle also ensures >90% cell viability after size-based sorting and synchronization of cell subpopulations. A summary of the various microfluidic cell cycle synchronization systems is presented in Table 2.

### Synchronization of human mesenchymal stem cells (hMSCs)

We next tested the ability of our device to synchronize primary cells, and specifically to synchronize human bone marrow derived mesenchymal stromal or stem cells (hMSCs).<sup>34</sup> These

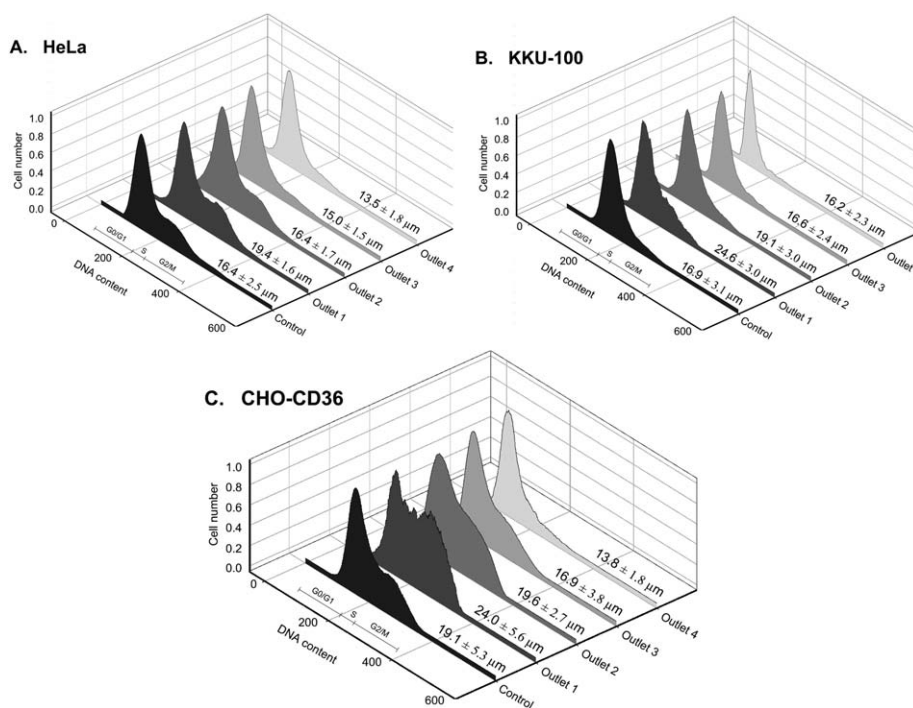


**Fig. 2** Cell cycle analysis results with permanent cell lines. Histogram indicating the distribution of the DNA content of the sorted singlet cells in the G0/G1, S and G2/M phase post synchronization. Cells in the G2/M phase have twice the amount of DNA than those in G0/G1 phase and hence double the fluorescence intensity. The larger cells collected from outlet 1 indicate an enrichment in the G2/M population, while the smaller cells collected from outlet 4 show significant enrichment of G0/G1 phase. The diameter (size) distributions of the synchronized cells are also indicated.

hMSCs differ from cancer cell lines or engineered cell lines in two important ways. First, the asynchronous cell population termed hMSCs is actually an enriched population of putative stem cells; the standard methods of purification of these rare cells from human bone marrow result in a broader distribution of cell diameter, morphology, and functionality than that is typical of a cell line or highly purified primary tissue cell.<sup>35,36</sup> Second, the hMSCs are highly susceptible to contact inhibition, such that expansion of hMSCs at low or high seeding density can alter the cell cycle and potentially the emergence of dominant subpopulations.<sup>37</sup> Our analysis of cellular DNA content for hMSCs seeded at densities of 1500 cm<sup>-2</sup> and 3000 cm<sup>-2</sup> indicates substantially fewer cells in the S and G2/M phases after two days

in culture (data not shown) as compared to fractions obtained for hMSCs seeded at a lower initial density. Thus, to enrich the S and G2/M populations, cells were seeded at a lower density of 500 cm<sup>-2</sup> and cultured for two days before sorting. Fig. 3 shows optical micrographs and viability results of the sorted hMSCs collected from outlets 1 through 4 using a 200 μm high channel. Following sorting, 3.8%, 31.2%, 44.9% and 20.1% of the initial asynchronous cell population were collected from outlets 1 through 4 respectively. The hMSCs collected from outlet 1 exhibited a mean cell diameter of 23.5 ± 5.6 μm and were significantly larger than those collected from outlet 4 (approximately 15.5 ± 2.1 μm). Following separation, cell viability was assessed *via* trypan blue exclusion assay and through long-term

**Table 1** Distribution of the sorted cells in the various cell cycle phase post synchronization

Cell type	Phase	Distribution%				
		Control	Outlet 1	Outlet 2	Outlet 3	Outlet 4
HeLa	G0/G1	70.0	55.0	56.0	79.0	84.0
	S	11.0	15.0	18.0	11.0	9.0
	G2/M	19.0	30.0	26.0	10.0	7.0
KKU-100	G0/G1	74.2	67.7	64.8	81.1	96.4
	S	15.4	13.3	20.5	11.9	2.3
	G2/M	10.4	19.0	14.7	7.0	1.4
CHO-CD36	G0/G1	55.0	37.0	43.0	62.0	86.0
	S	16.0	17.0	19.0	14.0	8.0
	G2/M	29.0	46.0	38.0	24.0	6.0
hMSCs	G0/G1	56.4	29.6	50.8	72.6	86.2
	S	16.6	19.8	17.8	12.0	5.9
	G2/M	27.0	50.6	31.4	15.4	7.9

**Table 2** Comparison of microfluidic separation techniques reported for cell cycle synchronization

Reference	Method	Separation principle	Separation type	Cell lines	Synchrony		
					G0/G1 purity	G2/M enrichment	Throughput
Kim <i>et al.</i> [14]	Dielectrophoresis	Inhomogeneous electric field	Active	MDA-MB-231	96%	$\sim 1 \times$ <sup>a</sup>	$2 \times 10^5$ cells per h
Thevoz <i>et al.</i> [15]	Acoustophoresis	Ultrasonic standing waves	Active	MDA-MB-231	84%	$23 \times$ <sup>a</sup>	$3 \times 10^6$ cells per h
Choi <i>et al.</i> [16]	Hydrophoresis	Inhomogeneous pressure field	Passive	U937	$\sim 96\%$	$3.7 \times$	$2.4 \times 10^5$ cells per h
Migita <i>et al.</i> [17]	Hydrodynamic filtration	Hydrodynamic force	Passive	HepG2	86%	$2.9 \times$	$3 \times 10^6$ cells per h
				NIH/3T3	81%	$3.6 \times$	
				MSCs	86%	$3.1 \times$	$15 \times 10^6$ cells per h
This work	Inertial	Lift forces and Dean drag	Passive	CHO-CD36	82%	$2 \times$	
				HeLa	84%	$2 \times$	
				KKU-100	96%	$2 \times$	

<sup>a</sup> Estimated from data presented in the paper.

re-culturing. The viability of the sorted cells was similar to that of the unsorted (control) hMSCs, with more than 90% of the cells collected from each outlets excluding the dye; this suggests that hMSCs were sorted without incurring gross physical damage (Fig. 3b and S2, ESI†). After 14 days of culture, the morphology of the sorted hMSCs was similar to that of the unsorted (control) cells, further demonstrating the maintenance of cell viability post-sorting (Fig. 3c).

In the unsorted, asynchronous (control) hMSC culture, 56.4% of the cells were in G0/G1, 16.6% in S and 27.0% in the G2/M phase, as shown by the DNA histogram (Fig. 4). Post synchronization, the cell population collected from outlet 1 comprised 70.4% of cells in the S and G2/M phases, while 86.2% of cells from outlet 4 were synchronized to the G0/G1 phase (Table 1). These results indicate that the G0/G1 to G2/M ratio of 3 : 1 for the asynchronous hMSC population is enriched to 16 : 1 for the hMSC subpopulation collected at outlet 4. Similarly, a fourfold enrichment in the G2/M population is achieved in the hMSC subpopulation collected at outlet 1. Although the cell cycle profiles indicate significant overlap between the outlets, the average cell size (diameter) collected from the four outlets shows significant difference ( $p < 0.05$ ). The overlap between adjacent outlets is attributed to the inherent heterogeneity in the size distribution between the various phases of the cell cycle.

To confirm that we were indeed synchronizing hMSCs in the G0/G1 phase, we compared the synchrony of the hMSCs subpopulations of smallest average diameter (from outlet 4) with the hMSCs arrested in the G0/G1 phase by means of serum starvation and contact inhibition (see Fig. S3, ESI†). We determined that 86.2% of the hMSCs collected from outlet 4 of our device were synchronized in the G0/G1 phase, which exceeded that achieved *via* contact inhibition (76.4%) and by 48 h serum starvation (77.5%); see Table S1, ESI†. The corresponding diameter distributions of the hMSCs collected from outlet 4 ( $15.5 \pm 2.1 \mu\text{m}$ ) narrowed as compared to serum starved ( $16.9 \pm 4.2 \mu\text{m}$ ) and contact inhibited ( $23.3 \pm 3.8 \mu\text{m}$ ) hMSCs. We note that contact inhibition produced cells with similar amount of DNA, but the cell size of the arrested population was as heterogeneous as in the unsorted asynchronous hMSCs population ( $21.9 \pm 3.5 \mu\text{m}$ ). While the main criterion for successful synchronization is that the DNA content in the synchronized cell subpopulation should be similar, the size distribution of the cells should also be relatively uniform as compared to the initial population distribution.<sup>33</sup> The wide variation in cell diameter of the contact-inhibited cells suggests that hMSCs were merely growth arrested with a similar amount of DNA, but that other cellular processes leading to protein and mass synthesis were not really synchronized. Conversely, withdrawal of serum from culture synchronized the hMSCs with G1 phase amount of DNA and arrested mass synthesis, but the cell diameter distribution was still relatively large as compared to G0/G1-enriched subpopulations synchronized by our device. We also note that the shape of serum starved hMSCs was more irregular and prone to membrane blebbing, suggesting that the normal physiology of the hMSCs was disrupted under serum starvation-induced stress.

We next investigated whether the hMSCs synchronized in this device would undergo synchronized divisions. The underlying assumption is that synchronized cells do not merely have similar diameters and DNA content, but that the cells are capable of

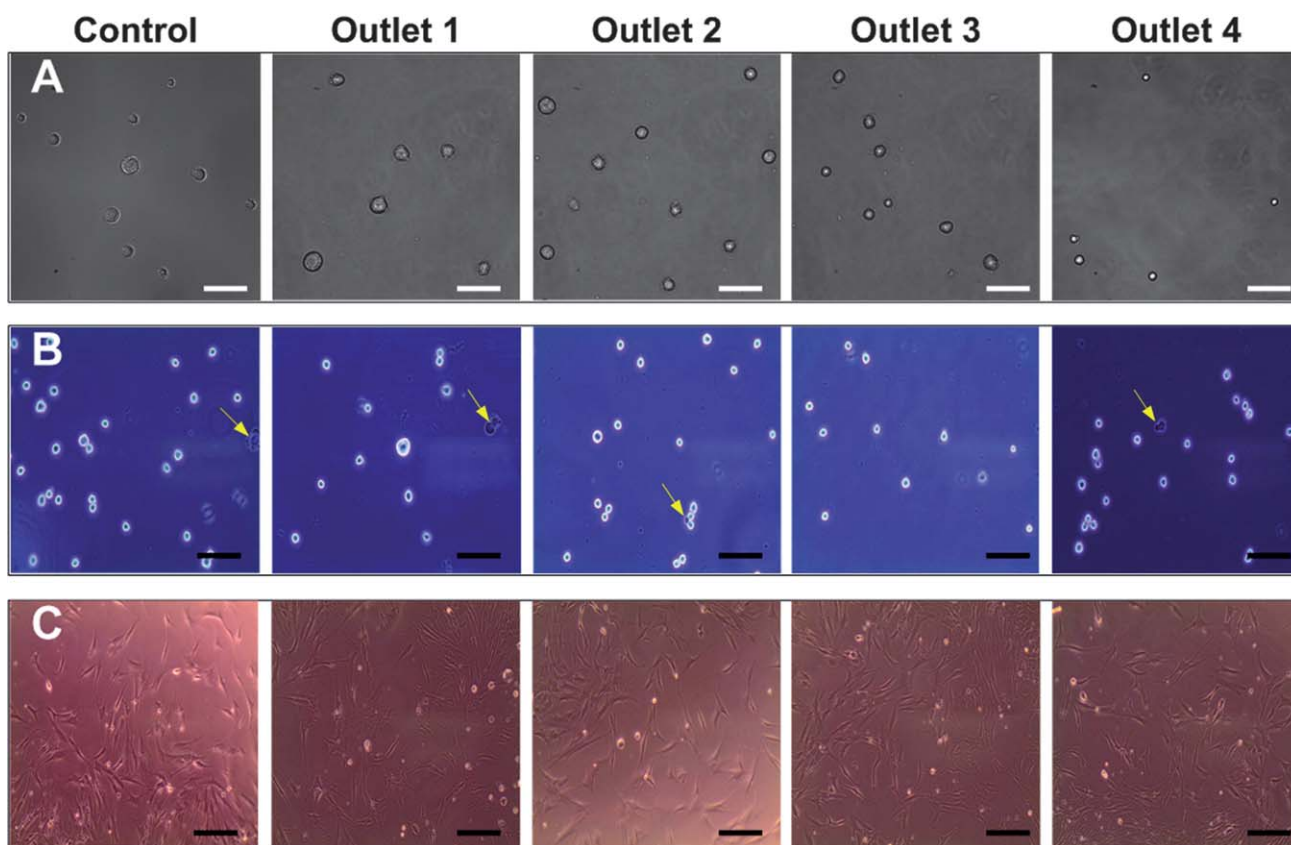


**Fig. 3** (A) Optical micrographs of the unsorted (control) and sorted hMSCs cells collected from outlets 1, 2, 3 and 4. The mean cell diameter collected at outlet 1 is  $\sim 24 \mu\text{m}$ , as compared to  $\sim 15 \mu\text{m}$  collected at outlet 4 ( $p < 0.001$ ). (B) Trypan-blue exclusion by collected cells indicates viability of hMSCs post sorting (arrows indicate non-viable cells). Results indicate that the high shear experienced by the cells in these microchannels do not compromise their viability, achieving  $>90\%$  cell recovery. (C) Optical micrograph of the re-seeded cells indicating no significant difference between the proliferation rates of cells collected from the outlets as compared to the unsorted population; this indicates high viability and sterility. Scale bar =  $50 \mu\text{m}$ .

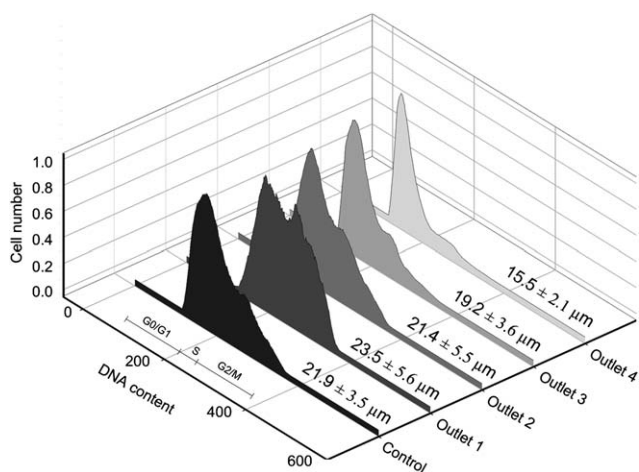


**Fig. 4** Histogram indicating the distribution of DNA content of the sorted hMSCs in the G0/G1, S and G2/M phase post synchronization. The diameter distributions of the synchronized cells are also indicated ( $p < 0.05$ ).

passing through the cell cycle as a relatively uniform cohort. To test this hypothesis, the hMSCs collected from outlet 4 with  $82\%$  of G0/G1 synchrony were replated and DNA content was

analyzed at 24, 48 and 72 h (Fig. 5). Interestingly, after 24 h of culture, the percentage of cells in the S and G2/M was  $79.8\%$ , indicating that most of the G0/G1 cells progressed through the subsequent phases (Table 3). Typically, mammalian cells reside in the G1/S phases for 16–24 h and only about 2–3 h in the G2/M phases.<sup>14</sup> It is therefore expected that the majority of the cells were found in the S and G2/M phases 24 h after culture. However, the synchrony of the cells decayed over time as a result of stochastic variation in interdivision times. The population of G0/G1 hMSCs increased to  $69.4\%$  after 74 h of culture, due at least in part to contact inhibition of cell growth. Many chemical methods or “batch treatments” (e.g., aphidicolin, roscovitine and colchicine) have been used to arrest cell cultures at a specific phase of the cell cycle. However, those chemical methods typically disrupt subsequent progression of the normal cell cycle progression.<sup>16</sup> For example, Whitfield *et al.* employed thymidine-nocodazole block to arrest HeLa cells in the G2 phase.<sup>38</sup> However, 12 hours after release from the arrest procedure, cells from all phases of the cell cycle were present rather than cells from only one or two phases. In contrast, our results show that hMSCs synchronized by our device exhibit relatively synchronized divisions over at least the next 24 h cycle.

Finally, we note that the cell cycle of hMSCs was correlated recently with a small and highly proliferative subpopulation of

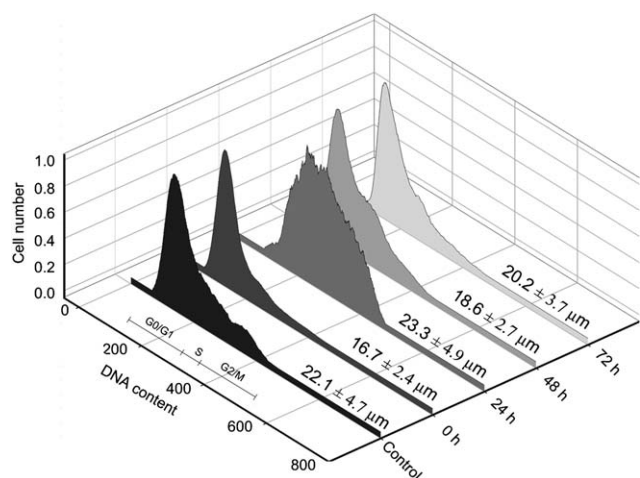


**Fig. 5** Histograms indicating the distribution of DNA content of the sorted hMSCs collected from outlet 4 at different increasing time intervals. The hMSCs demonstrate synchronized cell division as all the outlet 4 hMSCs (82.3% at 24 h) transit to S and G2/M phase at day 1 (79.7%). The percentage of cells in G0/G1 increases from day 2 onwards due to contact inhibition. The synchrony decays over time due to stochastic variations in the interdivision times. The cell cycle profile of the unsorted (control) hMSCs is also shown.

**Table 3** Distribution of the cell cycle phase of the replated human mesenchymal stromal or stem cells collected from outlet 4 of the spiral microchannel device, indicated at varying timepoints post synchronization

Phase	Control	Distribution (%)			
		0 h	24 h	48 h	72 h
G0/G1	64.5	82.3	19.7	51.9	69.4
S	23.2	14.3	45.2	34.7	23.9
G2/M	11.8	3.3	34.6	12.7	6.6

hMSCs; those smaller hMSCs further exhibited enhanced differentiation potential into typical mesenchymal tissue cell lineages *via* chemical induction.<sup>39</sup> Though beyond the scope of the current study, this demonstrated capacity to physically sort and collect viable cells as a function of cell diameter now enables future correlations among cell diameter and cell function in such heterogeneous cell populations.

## Conclusions

In this work, we demonstrate high-throughput and high-resolution separation of cell populations as a function of cell diameter *via* the application of a spiral microfluidic device. This approach employs the combined effect of inertial forces and Dean drag force to fractionate mammalian cells into different stages of the cell cycle on the basis of corresponding cell diameter. Distinct advantages of this platform over other microfluidic separation methods include continuous operation enabling significantly higher sample throughput ( $\sim 15 \times 10^6$  cells per h) and thus reduced sample processing time. The passive operating principle of flow-based physical sorting of cells eliminates the need to integrate external force fields for functionality or inhibitory

chemicals, and thereby preserves the integrity and viability of sorted cells (>90%). As mammalian cell suspensions can be separated and synchronized directly, direct modifications of the cells *via* molecular labeling steps is not required, further reducing processing time, cost, and potential modification of cell functionality post-sorting. This is the first demonstration of microfluidics enabling high-throughput cell cycle synchronization, while maintaining significantly higher viability for primary cells such as human mesenchymal stem cells. We believe that the simple, high-throughput and minimally disruptive nature of our device, which can be employed to fractionate cell subpopulations as a function of diameter and to synchronize the cell cycle, could find diverse applications in both basic and applied research.

## Acknowledgements

Support by the Singapore-MIT Alliance for Research and Technology (SMART) Centre (BioSyM IRG) is gratefully acknowledged. This work was carried out in part through the use of MIT's Microsystems Technology Laboratories. The KKU-100 cancer cells were received as a kind gift from Dr. Banchoop Sripa, Department of Pathology, The Liver Fluke and Cholangiocarcinoma Research Center, Khon Kaen University, Thailand.

## References

- 1 D. G. Johnson and C. L. Walker, *Annu. Rev. Pharmacol.*, 1999, **39**, 295–312.
- 2 J. Jolivet, K. H. Cowan, G. A. Curt, N. J. Clendeninn and B. A. Chabner, *N. Engl. J. Med.*, 1983, **309**, 1094.
- 3 J. Jackman and P. M. O'Connor, *Current Protocols in Cell Biology/Editorial Board*, Juan S. Bonifacino et al., 2001.
- 4 I. Wilmut, N. Beaujean, P. A. De Sousa, A. Dinnyes, T. J. King, L. A. Paterson, D. N. Wells and L. E. Young, *Nature*, 2002, **419**, 583–587.
- 5 M. H. Fox, R. A. Read and J. S. Bedford, *Cytometry*, 1987, **8**, 315–320.
- 6 M. J. Griffin, *In Vitro Cell. Devel. Biol. Plant*, 1976, **12**, 393–398.
- 7 R. W. Holley and J. A. Kiernan, *Proc. Natl. Acad. Sci. U. S. A.*, 1968, **60**, 300–304.
- 8 J. Gong, F. Traganos and Z. Darzynkiewicz, *Cell Growth Differ.*, 1995, **6**, 1485.
- 9 R. T. Schimke, A. L. Kung, D. F. Rush and S. W. Sherwood, *Cold Spring Harb. Symp. Quant. Biol.*, 1991, **66**, 417–425.
- 10 P. Van Vlasselaer, N. Falla, H. Snoeck and E. Mathieu, *Blood*, 1994, **84**, 753–763.
- 11 G. Banfalvi, *Nat. Protoc.*, 2008, **3**, 663–673.
- 12 L. K. Hohmann and T. B. Shows, *Somatic Cell Genet.*, 1979, **5**, 1013–1029.
- 13 A. A. S. Bhagat, H. Bow, H. W. Hou, S. J. Tan, J. Han and C. T. Lim, *Med. Biol. Eng. Comput.*, 2010, **48**, 999–1014.
- 14 U. Kim, C. W. Shu, K. Y. Dane, P. S. Daugherty, J. Y. J. Wang and H. T. Soh, *Proc. Natl. Acad. Sci. U. S. A.*, 2007, **104**, 20708.
- 15 P. Thevoz, J. D. Adams, H. Shea, H. Bruus and H. T. Soh, *Anal. Chem.*, 2010, **82**, 3094–3098.
- 16 S. Choi, S. Song, C. Choi and J. K. Park, *Anal. Chem.*, 2009, **81**, 1964–1968.
- 17 S. Migita, K. Funakoshi, D. Tsuya, T. Yamazaki, A. Taniguchi, Y. Sugimoto, N. Hanagata and T. Ikoma, *Anal. Methods*, 2010, **2**, 657–660.
- 18 A. A. S. Bhagat, S. S. Kuntaegowdanahalli and I. Papautsky, *Microfluid. Nanofluid.*, 2009, **7**, 217–226.
- 19 D. Di Carlo, D. Irimia, R. G. Tompkins and M. Toner, *Proc. Natl. Acad. Sci. U. S. A.*, 2007, **104**, 18892.
- 20 Y. Xia and G. M. Whitesides, *Annu. Rev. Mater. Sci.*, 1998, **28**, 153–184.
- 21 J. Koo and C. Kleinstreuer, *J. Micromech. Microeng.*, 2003, **13**, 568.

- 
- 22 P. Wersto, F. J. Chrest, J. F. Leary, C. Morris, M. A. Stetler-Stevenson and E. Gabrielson, *Cytometry*, 2001, **46**, 296–306.
- 23 S. S. Kuntaegowdanahalli, A. A. S. Bhagat, G. Kumar and I. Papautsky, *Lab Chip*, 2009, **9**, 2973–2980.
- 24 A. Russom, A. K. Gupta, S. Nagrath, D. D. Carlo, J. F. Edd and M. Toner, *New J. Phys.*, 2009, **11**, 075025.
- 25 G. Segre, *Nature*, 1961, **189**, 209–210.
- 26 G. Segre and A. Silberberg, *J. Fluid Mech.*, 1962, **14**, 115–135.
- 27 J. P. Matas, J. F. Morris and E. Guazzelli, *J. Fluid Mech.*, 2004, **515**, 171–195.
- 28 B. Chun and A. J. C. Ladd, *Phys. Fluids*, 2006, **18**, 031704.
- 29 R. E. Hampton, A. A. Mammoli, A. L. Graham, N. Tetlow and S. A. Altobelli, *J. Rheol.*, 1997, **41**, 621.
- 30 E. S. Asmolov, *J. Fluid Mech.*, 1999, **381**, 63–87.
- 31 A. A. S. Bhagat, S. S. Kuntaegowdanahalli and I. Papautsky, *Phys. Fluids*, 2008, **20**, 101702.
- 32 A. A. S. Bhagat, S. S. Kuntaegowdanahalli and I. Papautsky, *Lab Chip*, 2008, **8**, 1906–1914.
- 33 S. Cooper, *Cell. Mol. Life Sci.*, 2003, **60**, 1099–1106.
- 34 W. C. Lee, A. A. S. Bhagat, S. Huang, K. J. Van Vliet, J. Han and C. T. Lim, in *14th International Conference on Miniaturized Systems for Chemistry and Life Sciences*, Groningen, The Netherlands, 2010, pp. 209–211.
- 35 P. Bianco, P. G. Robey and P. J. Simmons, *Cell Stem Cell*, 2008, **2**, 313–319.
- 36 J. M. Maloney, D. Nikova, F. Lautenschläger, E. Clarke, R. Langer, J. Guck, K. J. Van Vliet, *Biophys. J.*, 99, 2479–2487.
- 37 D. J. Prockop, *Mol. Ther.*, 2009, **17**, 939–946.
- 38 M. L. Whitfield, G. Sherlock, A. J. Saldanha, J. I. Murray, C. A. Ball, K. E. Alexander, J. C. Matese, C. M. Perou, M. M. Hurt and P. O. Brown, *Mol. Biol. Cell*, 2002, **13**, 1977–2000.
- 39 D. C. Colter, I. Sekiya and D. J. Prockop, *Proc. Natl. Acad. Sci. U. S. A.*, 2001, **98**, 7841.